Journal of Magnetism and Magnetic Materials 468 (2018) 91–99

Contents lists available at ScienceDirect

Journal of Magnetism and Magnetic Materials

journal homepage: www.elsevier.com/locate/jmmm

Research articles

Phase separation in Fe-Ti-Al alloy – Structural, magnetic, and Mössbauer study

Y. Jiraskova[a,*], N. Pizurova[a], A. Titov[b,c], D. Janickovic[d], M. Friak[a]

[a] Institute of Physics of Materials, AS CR, Zizkova 22, 616 620 Brno, Czech Republic
[b] Department of Physics, VSB-Technical University of Ostrava, 17, Listopadu 15, 708 33 Ostrava-Poruba, Czech Republic
[c] CEITEC IPM, Institute of Physics of Materials, AS CR, Zizkova 22, 616 62 Brno, Czech Republic
[d] Institute of Physics, Slovak Academy of Sciences, Dubravska cesta 9, 845 11 Bratislava, Slovakia

ARTICLE INFO

Keywords:
Fe-Al-Ti alloy
Structural properties
Magnetic properties
Mössbauer spectrometry

ABSTRACT

The influence of Ti substituting partially Fe in Fe – 22 at.% Al alloy on the structure and magnetic properties is investigated experimentally by electron microscopy, X-ray diffraction, Mössbauer spectrometry, and by magnetic measurements at room and low temperatures. The samples in a form of discs prepared by cutting the arc-melted button-type ingots have yielded a coarse-grained structure in the Fe – 22 at.% Al sample and fine Fe-Al-Ti cuboids embedded in Fe-Al(Ti) matrix in the Fe – 22 at.% Al – 7 at.% Ti alloy. The mean cuboids' size was 45 nm and the mean composition was determined to be close to Fe_2TiAl. The as-prepared Fe-Al-Ti samples exhibited substantially reduced saturation magnetization and markedly higher remanent magnetization and coercivity as compared to the as-prepared Fe-Al sample. The thermal treatment of the Fe-Al sample at 1073 K/168 h has changed its magnetic behaviour only slightly, whereas the treatment of the Fe-Al-Ti sample at 1273 K/168 h resulted in remarkable softening of its magnetic properties.

1. Introduction

Fe-Al alloys have been intensively investigated for many years because of their excellent oxidation resistance discovered around 1930, similarly excellent sulphidation resistance, and a potentially lower cost compared to other materials used in high-temperature applications. They are featured also by a low density being about 30% lower in comparison to high-temperature structural materials as Ni-based superalloys or stainless steels. However, for practical applications, the workability and the transition temperature from the ductile to brittle fracture need to be improved.

It is known that the mechanical as well as magnetic properties of the Fe-Al alloys depend strongly on deviation of composition from the stoichiometry and on a degree of order. In the phase diagram of the Fe-Al binary system in Fig. 1 there are two kinds of 2nd-order order-disorder transitions in the α-Fe phase region, A2/B2 and B2/$D0_3$, and two kinds of phase separations, (A2 + B2) and (A2 + $D0_3$). The main structural units are depicted on the right from the phase diagram. The order-disorder transitions as well as the phase separations can be affected by the addition of a third alloy component and by finding a suitable thermal treatment. The majority of studies is devoted to effects of alloying elements, e.g., Ti, Co, Cr, Nb, Si, Mo, etc., substituting either Fe atoms or Al atoms in the Fe-Al matrix in various concentrations on the microstructure and the phase separation related, in particular, to mechanical properties [1–8]. From the magnetic viewpoint the attention concentrates mainly on Co, Mo, Si, and Nb. The Fe-Si-Al alloys with $D0_3$ ($L2_1$) structure are commercially known as SENDUST soft magnetic material [9]. The addition of Mo to Fe-Al using conventional technology has been found to slightly improve mechanical properties [10] and to positively influence magnetic properties [11–13]. Not too much is known about an influence of cobalt and niobium present as the third element in Fe-Al and presently a higher interest is devoted to addition of titanium that should contribute to improving of predominantly mechanical behaviour of the Fe-Al and/or Al-Fe alloys [14–16]. This improvement consists in the stabilization of the $D0_3$ ordered structure and in an expansion of the (A2 + $D0_3$) phase field [17]. The $D0_3$ phase in Fe-Al-Ti system is denoted as $L2_1$ and it corresponds to Fe_2TiAl. The existence of coherent $L2_1$ and A2 phases can contribute to strengthening of Fe-Al based alloys as indicated also by the quantum-mechanical calculations [18]. The influence of such structure on electrical and/or magnetic properties is not sufficiently studied. Therefore, series of Fe-22 at.% Al alloys with 5, 7, and 8 at.% Ti was prepared. The most prospective from a structural viewpoint was the alloy with 7 at.% Ti substituting iron. Therefore, it was chosen for the present investigation

* Corresponding author.
E-mail address: jirasko@ipm.cz (Y. Jiraskova).

https://doi.org/10.1016/j.jmmm.2018.07.065
Received 17 April 2018; Received in revised form 21 June 2018; Accepted 21 July 2018
Available online 23 July 2018

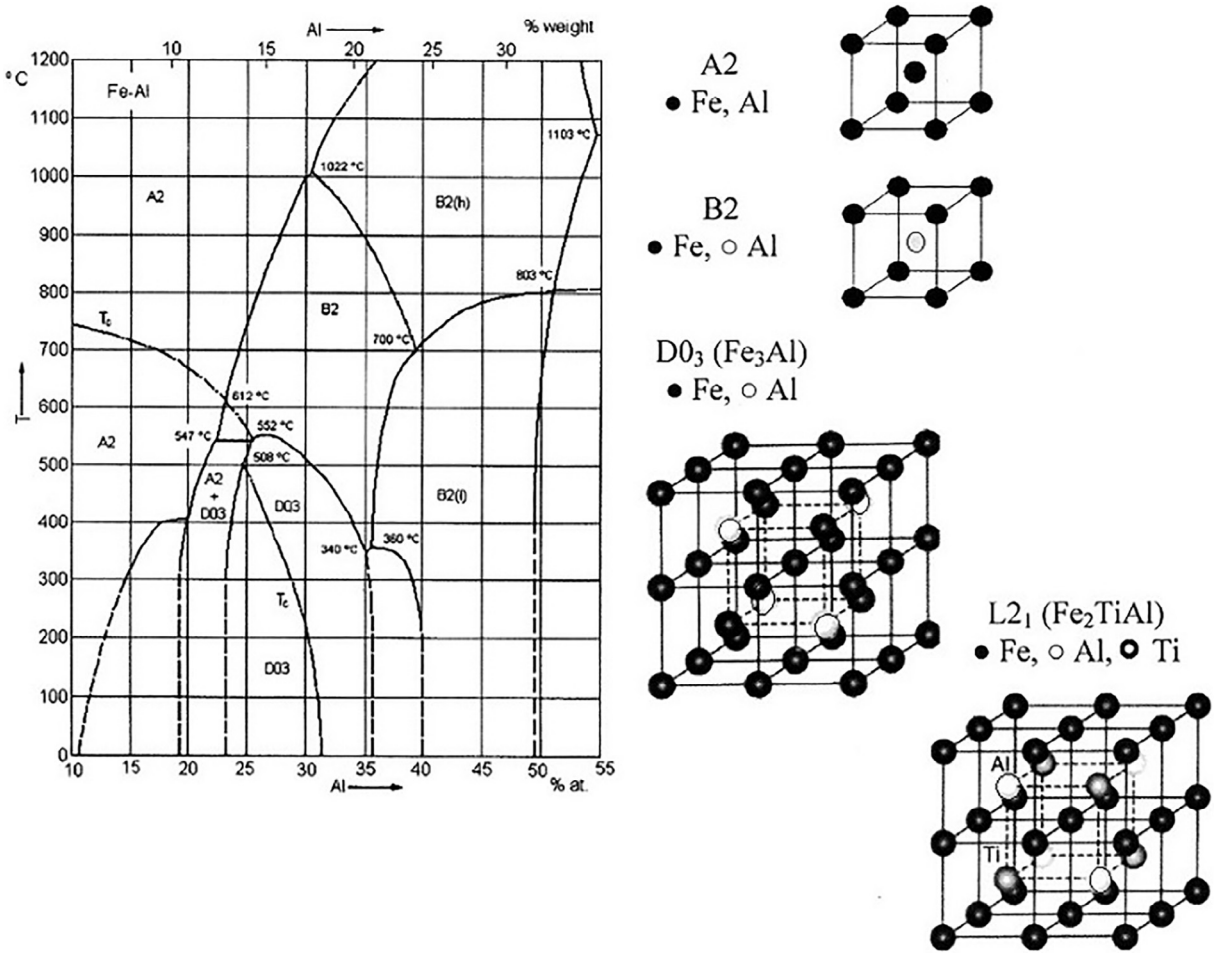

Fig. 1. Fe-Al phase diagram and corresponding atoms ordering in three structural units.

simultaneously with the pure Fe – 22 at.% Al alloy. The main attention is devoted to the effect of the paramagnetic Fe_2TiAl ($L2_1$) embedded in the Fe-Al (A2) ferromagnetic matrix on selected magnetic properties.

2. Experimental details

2.1. Sample preparation

Both alloys were prepared from high-purity elements; Fe – 99.95%, Ti – 99.8%, and Al – 99.95%. Arc melting using a MAM-1 furnace (Buehler GmbH) was used for the production of button-type ingots. Each ingot was re-melted four times under Ar (4N8) of 350 mbar (35 kPa) pressure to guarantee a good chemical homogeneity. Then the ingots were cut using spark erosion in deionized water into discs about 500 μm thick and 18 mm in diameter. The surface of the disc-samples, denoted FA (Fe-Al alloy) and FAT (Fe-Al-Ti alloy), was ground and polished to remove oxides and polished using Vibromet for 24 h to guarantee the best possible surface smoothness. Both samples were investigated in the as-prepared state and after heat treatment corresponding to chemical composition: the FA sample at 1073 K (FA-a) and the FAT sample at 1273 K (FAT-a), both for 168 h in Ar atmosphere with a subsequent furnace-cooling down to room temperature (RT).

3. Experimental methods

3.1. Scanning and transmission electron microscopy (SEM, TEM)

A TESCAN LYRA 3XMU FEG/SEM scanning electron microscope working at accelerating voltage of 20 kV equipped with an XMax80 Oxford Instruments detector for energy dispersive X-ray analysis (EDX) was used to follow the chemical composition. The cross sections of the samples were shortly chemically etched in Nital prior the SEM observations.

A Jeol JEM 2100F HRTEM with a Schottky cathode operating at 200 kV was used to study microstructural details. The samples were prepared by grinding of 500 μm thick disc from both sides to a thickness about 100 μm using abrasive SiC papers of various grit sizes. Samples of 3 mm in diameter were punched from this foil and furthermore thinned using the standard double-jet technique in a Tenupol polishing machine.

3.2. X-ray diffraction (XRD)

An X'PERT PRO diffractometer (Panalytical) in the symmetric Bragg-Brentano geometry with Co Kα radiation ($\lambda = 0.17902$ nm) was used to study the structural and compositional properties. The X-ray diffractograms were measured at room temperature (RT) in the range of 2Θ from 35° to 135° in steps of 0.01° and 500 s per deg. The analysis of patterns was realized by HighScore Plus program using the Rietveld structure refinement method [19] and the ICSD database of inorganic and related structures [20]. Besides the lattice parameters of analyzed phases, the size of coherently diffracting domains was obtained from the pattern analysis.

3.3. Magnetic measurements

RT bulk hysteresis loops and thermomagnetic curves (TMC) in an external magnetic field of 400 kA/m and vacuum, temperature increase

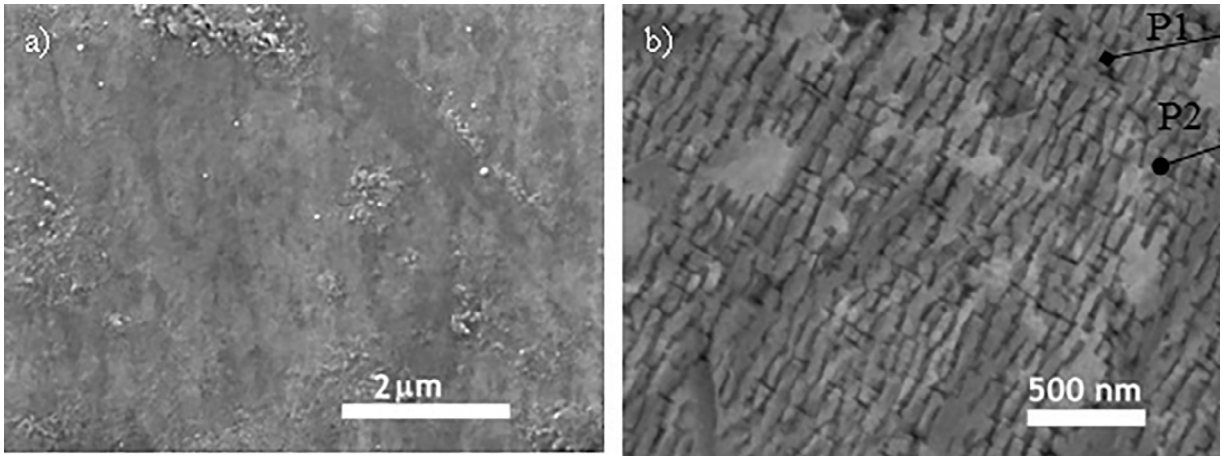

Fig. 2. Cross section morphology of the as-prepared samples: a) $Fe_{78}Al_{22}$ (FA), b) $Fe_{71}Al_{22}Ti_7$ (FAT).

4 K/min, were measured using a vibrating sample magnetometer (VSM) EG&G Princeton Applied Research Corporation. The magnetic characteristics, coercivity, remanent and saturation magnetizations were derived from the hysteresis loops with the accuracy of ± 1%. The zero-field-cooled (ZFC) and field-cooled (FC) curves in the external fields of 8 kA/m and 80 kA/m as well as the hysteresis curves at selected low temperatures (LT) were obtained using a Physical Property Measuring System (PPMS) to complete the RT magnetic data.

3.4. Mössbauer spectrometry (MS)

^{57}Fe Mössbauer spectrometry was used to gain insight into the structural evolution of the local environment of iron atoms. The measurements were carried out at RT using a ^{57}Co(Rh) source in scattering geometry by detecting γ-rays with depth sensitivity of about 30 µm. The calibration of velocity scales was performed with α-Fe and the isomer shifts are given with respect to the RT Mössbauer spectrum of α-Fe. All spectra were evaluated within the transmission integral approach using the CONFIT program package based on a non-linear least-squares procedure with the Fast Fourier Transform technique. A combination with an improved matrix formalism can create various physical models to analyze the measured experimental data in a proper way [21]. In the measured Mössbauer spectrum the crystalline components are represented by discrete single-, double-, and/or six-line Lorentzian subspectra determined by discrete values of hyperfine parameters, δ – isomer shift(s), Δ – quadrupole splitting(s), and B – hyperfine induction (s), corresponding to paramagnetic (pmc) and/or ferromagnetic (fmc) phases, respectively. All components are further described by their intensities, A.

Moreover, the experimental data of the Fe-Al sample in both states were analyzed also by fitting to models of the structure atomic order. The individual superstructures were divided into sublattices, for which the content of non-iron atoms was controlled by the ordering parameters. The distribution of "impurity" atoms within individual sublattices was supposed to be random and the binomial distribution function was used:

$$p_i(j, x) = \binom{i}{j} \cdot x^j (1-x)^{i-j} \quad (1)$$

Here, i is the number of atoms in the given coordination sphere (the calculations were limited to two coordination spheres), j is the number of impurity atoms, x is the impurity concentration within the particular sublattice, and $p_i(j,x)$ denotes the corresponding probability. Besides the disordered structure $A2$, the combination of $A2$ and DO_3 order (four sublattices and two ordering parameters) could be supposed [22]. As it concerns the individual components of Mössbauer spectra, the reduction of hyperfine induction with increasing number j of impurity Al atoms was supposed to be quadratic in the first coordination sphere and linear in the second one. The analogical influence on the isomer shift was set to be linear for both coordination spheres. Principally, the effect of all atoms on both hyperfine field and isomer shift is additive from the physical viewpoint. However, the restriction of the calculations to first two coordination spheres and the volume effects omission lead to necessity to approximate empirically the influence of the nearest neighbours on the hyperfine field – where the effect is the strongest – with a slightly bent curve instead of the straight line (a quadratic function instead of a linear dependence) [23]. This effect is yet more pronounced for higher Al atomic concentrations. Quadrupole splitting and correlation effects were neglected. The intensity of Mössbauer sextuplets representing an individual configuration was fitted as linearly dependent on the computed probability. In such a way, except the intensity/probability coefficient, ordering parameters can be obtained with coefficients describing dependences of the hyperfine induction and the isomer shift. The application of this simulation has allowed us to compare its results with those obtained using CONFIT.

4. Results and discussion

4.1. Microstructure and chemical composition

4.1.1. Scanning electron microscopy

The content of elements was checked by EDX from the areas of about 1 mm^2. The distribution of elements was homogeneous and resulted in the following average values: (77.1 ± 0.2) at.% Fe – (22.9 ± 0.2) at.% Al at the FA sample, (70.2 ± 0.2) at.% Fe – (22.6 ± 0.2) at.% Al – (7.2 ± 0.1) at.% Ti at the FAT sample. These results are in good agreement with the nominal compositions.

The polished cross section microstructures of both samples in the as-prepared state (FA and FAT) are shown in Fig. 2. The irregular grains are observed at the FA sample in Fig. 2a. A very fine-scale coherent two-phase microstructure was formed by an addition of Ti into Fe-Al alloy as seen in Fig. 2b. The small cuboids-type sub-grains of a phase P1 are aligned nearly at a single direction and separated by the grain boundaries of a phase P2. Similar structure was observed, e.g., for Fe-20.4 at.% Al-0.06 at.% Hf-3.8 at.% Mo-8.3 at.% Ti [1], Fe-22 at.% Al-7 at.% Ti [24], or in Fe-Al alloys with Ti content greater that 5 at.% and referred to as a "basket weave" by Sellers et al. [25]. The annealing at appropriate temperatures has contributed to a grain enlargement and the additional etching has allowed us to highlight the structure in both samples as seen in Fig. 3a and b.

The needle shape structure of sub-grains is visible in the FA-a sample (Fig. 3a) and the larger cuboids of the approximate Fe_2TiAl

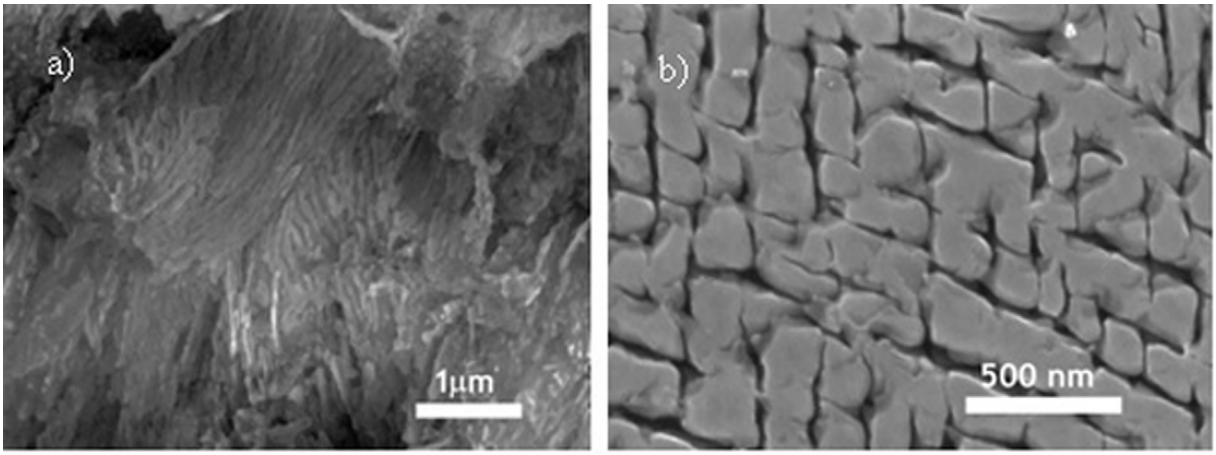

Fig. 3. Cross section morphology of the annealed samples: a) $Fe_{78}Al_{22}$ – 1073 K/168 h (FA-a), b) $Fe_{71}Al_{22}Ti_7$ – 1273 K/168 h (FAT-a).

composition (Fig. 3b) are seen in the FAT-a. The chemical analysis has shown that the intergrain regions are mainly composed of Fe-Al but with traces of Ti which cannot be fully excluded and therefore this phase is denoted Fe-Al (Ti) in the next text.

4.1.2. Transmission electron microscopy

Transmission electron microscopy (a) and corresponding high resolution TEM (HRTEM) images (b) for the as-prepared FA are shown in Fig. 4. The TEM image of cuboids formed in the as-prepared FAT sample and well visible grain boundaries are shown in Fig. 5. The HRTEM images of two sub-grains and their processing by a Fast Fourier Transformation method shown in Fig. 6 have confirmed the same composition and the identical orientation in both sub-grains.

4.2. X-ray diffraction

The X-ray diffraction patterns of the as-prepared samples (FA, FAT) are seen in Fig. 7. The Fe-Al phase was analysed using ICSD 107805 for the 229 (Im3-m) space group and using ICSD 607484 for the 225 (Fm-3 m) space group. In the case of the Fe_2TiAl ($L2_1$) phase the ICSD 57827 data sheet was applied. The parameters obtained using HighScore Plus program including Rietveld analysis, i.e., the weight phase content (*RA*), the lattice parameter (*a*), and the mean microdomain size (d_{mean}) are summarized in Table 1. The microdomain size calculations were done using the Scherrer formula for the peak's (0 2 2) and (0 1 1) positions around $2\theta \sim 51°$.

A disordered A2 structure dominates in the as-prepared state of the

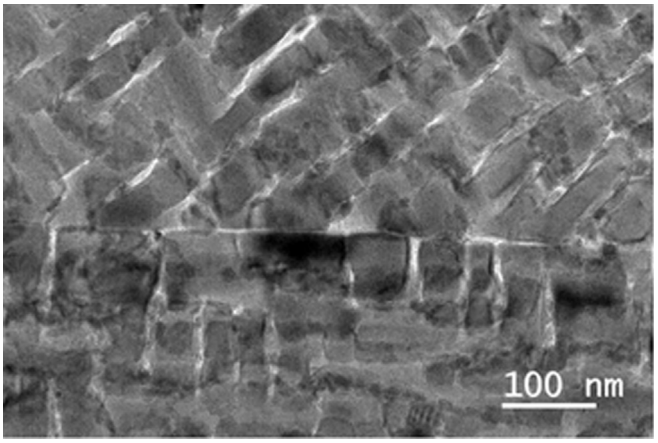

Fig. 5. TEM pattern of the as-prepared $Fe_{71}Al_{22}Ti_7$ (FAT) sample with well visible grain boundaries.

$F_{78}A_{22}$ (FA) sample. The thermal treatment at 1073 K/168 h followed by slow cooling has contributed to an increase of $D0_3$-ordered portion in the FA sample and to a slight increase in the mean crystallite size.

The pattern of the Fe-Al-Ti has confirmed a presence of the Fe_2TiAl phase as observed by SEM (Fig. 2b) besides the Fe-Al phase. Nevertheless, the patterns of both phases are very similar. After the annealing at 1273 K/168 h the patterns of both phases were not reliably

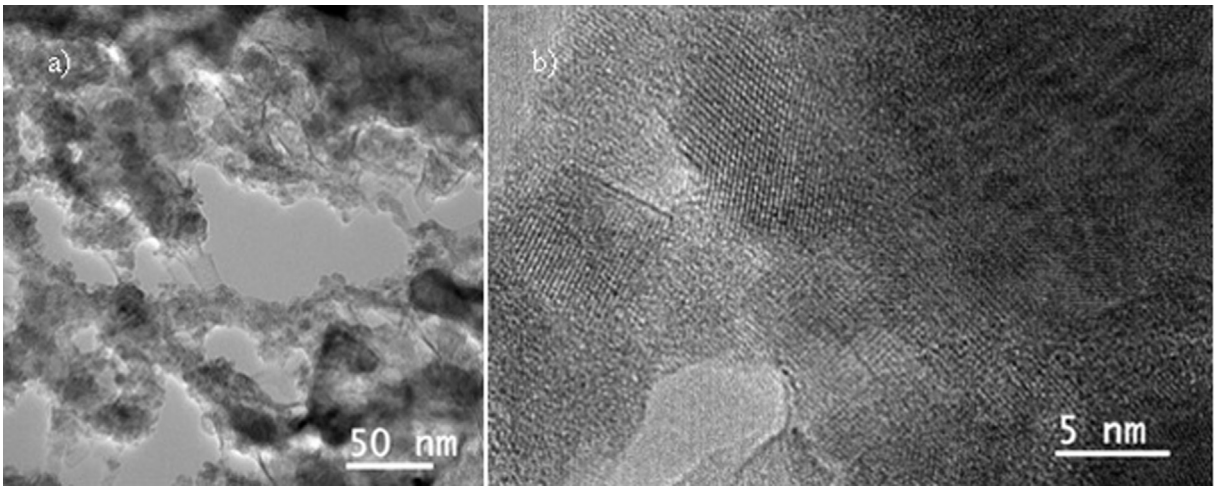

Fig. 4. TEM (a) and HRTEM (b) patterns of the as-prepared $Fe_{78}Al_{22}$ (FA) sample.

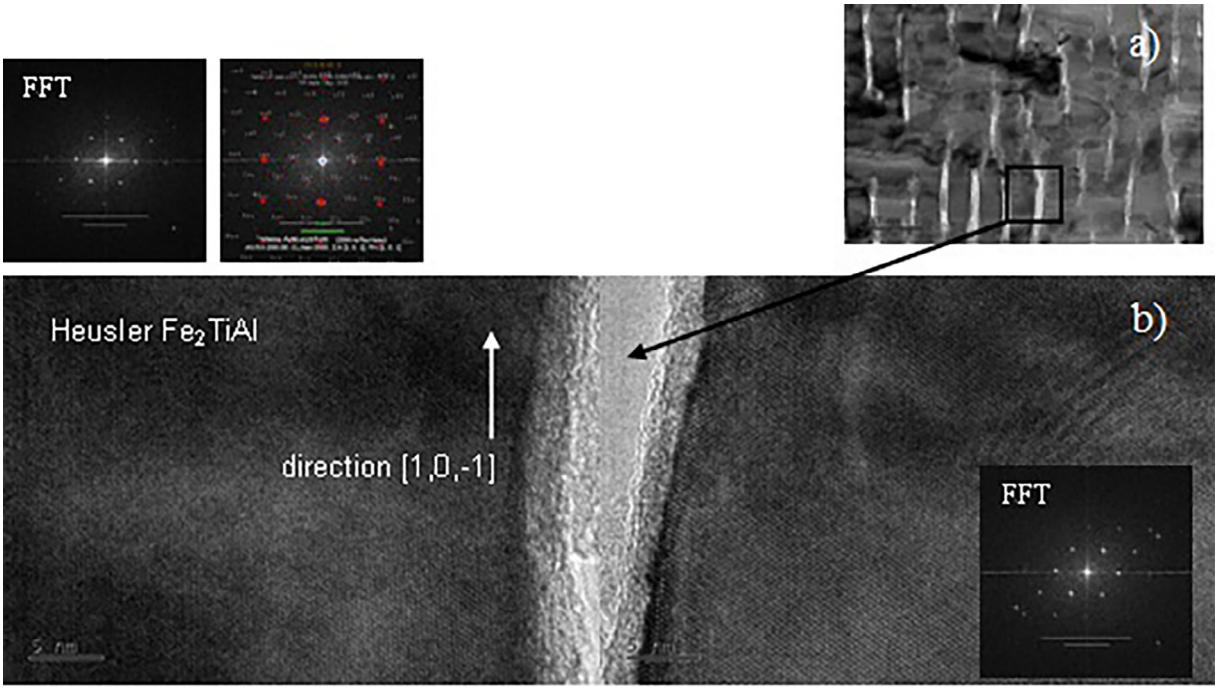

Fig. 6. TEM (a) and HRTEM (b) patterns of the as-prepared $Fe_{71}Al_{22}Ti_7$ (FAT) sample.

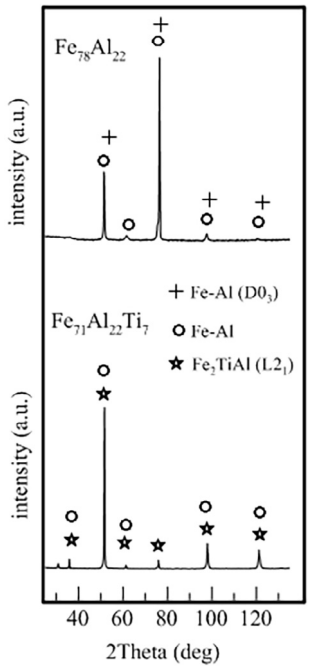

Fig. 7. X-ray patterns of Fe-Al (FA) and Fe-Al-Ti (FAT) samples in the as-prepared state.

distinguishable and the data in Table 1 represent the $L2_1$ structure of the Fe_2TiAl by supposing the minor portion of the Fe-Al(Ti) phase. The crystallite size in the FAT-a sample (Table 1) is approximately ten times higher than that in the FAT sample which is in agreement with the morphology seen in Fig. 3b.

The lattice constants listed in Table 1 are in relatively good agreement with those presented by other authors. For example A. Michalcova et al. [15] presented for a Fe-22Al-5Ti alloy the lattice constant for the A2 structure 0.289 nm and for the $L2_1$ structure 0.584 nm, about 0.581 nm for the same structure is presented in Ref. [14], theoretical calculation [26] yielded for the $L2_1$ structure 0.579 nm, Shreder et al. [18] have prepared and studied Fe_2TiAl with $L2_1$ structure and lattice parameter 0.5858 nm, Brzakalik et al. [27] have presented for Fe_2TiAl the value slightly above 0.587 nm, and Buschow et al. [28] have found the lattice parameter of Fe_2TiAl equal to 0.5879 nm.

Table 1
The results of the Rietveld analysis: phase content, *RA*, lattice parameter, *a*, and mean microdomain size, d_{mean}, obtained for the as-prepared $Fe_{78}Al_{22}$ (FA) and $Fe_{72}Al_{22}Ti_7$ (FAT) samples, and the annealed samples FA-a (1073 K/168 h) and FAT-a (1273 K/168 h).

sample	phase	*RA* (wt. %)	*a* (nm)	d_{mean} (nm)
FA	*A2*	87.4	0.2911(2)	26.6
	$D0_3$	12.6	0.5785(3)	
FA-a	*A2*	56.7	0.2922(3)	32.3
	$D0_3$	43.3	0.5813(3)	
FAT	*A2*	32.0	0.2903(1)	45.2
	$L2_1$	68.0	0.5806(1)	
FAT-a	$L2_1(D0_3)$	100.0	0.5809(1)	457.4

4.3. Magnetic measurements

The room-temperature magnetic characteristics summarized in Table 2 were derived from the hysteresis loops and thermomagnetic curves (TMC) in Fig. 8, measured for all samples using VSM. The values of the Curie temperature, T_C, were determined for all samples as inflection points on the thermomagnetic curves, illustrated for the FA

Table 2
Magnetic parameters derived from the room-temperature hysteresis loops: saturation and remanent magnetizations, M_s, M_r, coercivity, H_c, and Curie temperature, T_C, determined as mean values from the thermomagnetic curves (heating/cooling).

Sample	FA	FA-a	FAT	FAT-a
M_s (Am^2kg^{-1})	174.69	179.49	84.55	99.98
M_r (Am^2kg^{-1})	0.88	0.64	13.57	0.91
H_c (kA/m)	0.94	0.58	15.65	0.89
T_C (K)-heating/cooling	907	929	929	933

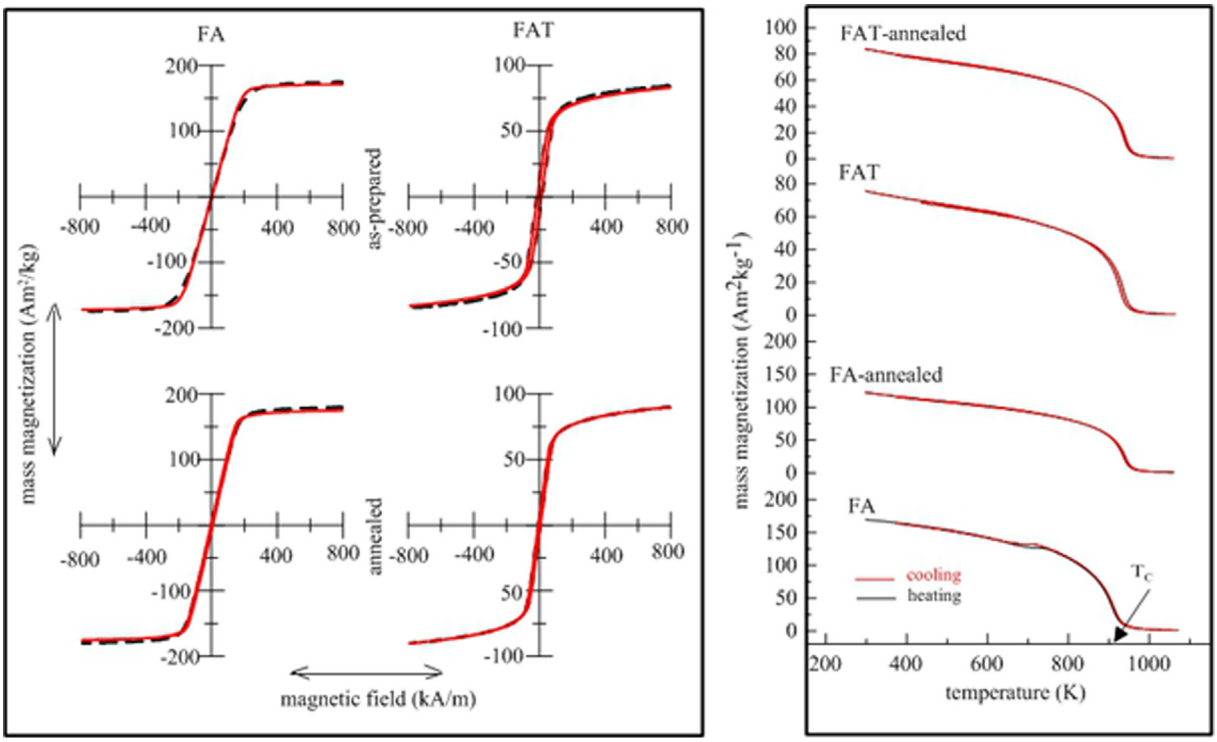

Fig. 8. Hysteresis loops (left) and thermomagnetic curves (right) for the $Fe_{78}Al_{22}$ and $Fe_{71}Al_{22}Ti_7$ samples in the as-prepared (FA, FAT) and annealed (FA-a, FAT-a) states.

sample in Fig. 8, using a numerical analysis of measured experimental data. The T_C in case of the samples modified by Ti (FAT, FAT-a) represents a ferro-/paramagnetic transition of the bcc-Fe-Al(Ti) intergrain phase because the Heusler Fe_2TiAl phase is in a paramagnetic state above RT. The slightly higher T_C values can be influenced by presence of the small Ti content evidenced by SEM.

Based on the polynomial dependence of T_C on aluminium concentration presented by Stein and Palm [29] the Curie temperature of 907 K determined for the FA sample corresponds well to an alloy with nearly 22 at.% Al. It is slightly below the value determined by EDX mentioned above. The annealing of this sample has contributed to improvement of the magnetic parameters, M_s, M_r, and to the magnetic softening (lowering H_c) due to an annealing out of defects and stresses in the sample. The higher value of T_C after annealing reflects the complicated magnetic behaviour of α-Fe-Al alloys, in the concentration region of (22–25) at.% Al. It is due to a higher contribution of the $D0_3$ type structure yielding different magnetic interactions between nearest neighbouring iron atoms and between iron atoms separated by an aluminium atom [30].

Pronounced differences of magnetic parameters due to the annealing are seen for the Fe-Al-Ti samples. The high and low values of the coercivity and remanent magnetization at the FAT and FAT-a samples, respectively, can be understood in part by the grain size effect as documented by the well-known dependence of the coercivity on the grain size [31]. If the average grain size is small enough (< 30 nm) and/or large (> 50 μm) then the coercivity is low. According to SEM observations, the present samples consist of the large grains of mainly Fe-Al composition and small Fe-Al-Ti cuboids, both influencing the magnetic characteristics due to their different magneto-crystalline and magneto-elastic anisotropies. The annealing has contributed to the magnetic softening and increase in saturation magnetization (FAT-a in Table 2). The visible lowering of the M_r and H_c is connected with a marked change in the grain size (about ten times higher size of cuboids) and the higher M_s reflects the higher portion of the ferromagnetic intergrain phase. The value is slightly higher as compared to 97 Am^2/kg presented for Fe_3Al + 5 at.% Ti by Sellers et al. [25]. For the same alloy the authors suppose a coexistence of two distinct magnetic phases which is reflected by two values of the Curie temperature, namely 250/660 °C, in their magnetization curve. For the sample Fe_3Al + 7 at.% Ti they present T_C = 692 °C (965 K) which is, vice versa, slightly higher than obtained by present measurements (Table 2). As it was mentioned above, it reflects the complicated magnetic behaviour of also ternary Fe-Al-X alloys at Al concentrations between 22 and 25 at.% influenced by the degree of ordering and thereby by the nearest neighbour configurations of Fe atoms [25,30,32–33].

Besides the RT magnetic measurements, the low-temperature dependences of the magnetization and hysteresis loops were measured for FAT and FAT-a samples and the results are summarized in Fig. 9. While the coercivity and remanent magnetization do not show any important changes at decreasing temperature, the saturation magnetization increases yielding the same trend for FAT and FAT-a (Fig. 9 left panel). The ZFC and FC curves measured for both, FAT and FAT-a, samples in the 8 kA/m and 80 kA/m external fields, are shown in Fig. 9 right panel. The maximum on the ZFC curve, so called mean blocking temperature, corresponds to the most probable size of magnetic nanoparticles in a given assembly. On the other hand, the temperature at which the ZFC and FC curves separate is the temperature of irreversibility which represents the blocking temperature of the largest particles in the assembly. Both temperatures are well detectable at the low-temperature dependences of magnetizations for both external fields at the FAT sample. The FC curves below the blocking temperature are nearly constant reflecting strong interactions among particles and corresponding to presence of the ferromagnetic Fe-Al(Ti) phase.

Different dependences are seen for the annealed FAT-a sample. An increase in mass magnetization already above RT indicates presence of an additional magnetic phase being weakly ferromagnetic or antiferromagnetic and additive to the fmc Fe-Al(Ti) phase. Its magnetic transition temperature is slightly above 200 K. This value is substantially higher as compared to 108 K for Fe_2TiAl phase [34]. Speculatively this could reflect a formation of clusters of a Ti(Fe,Al) Laves phase.

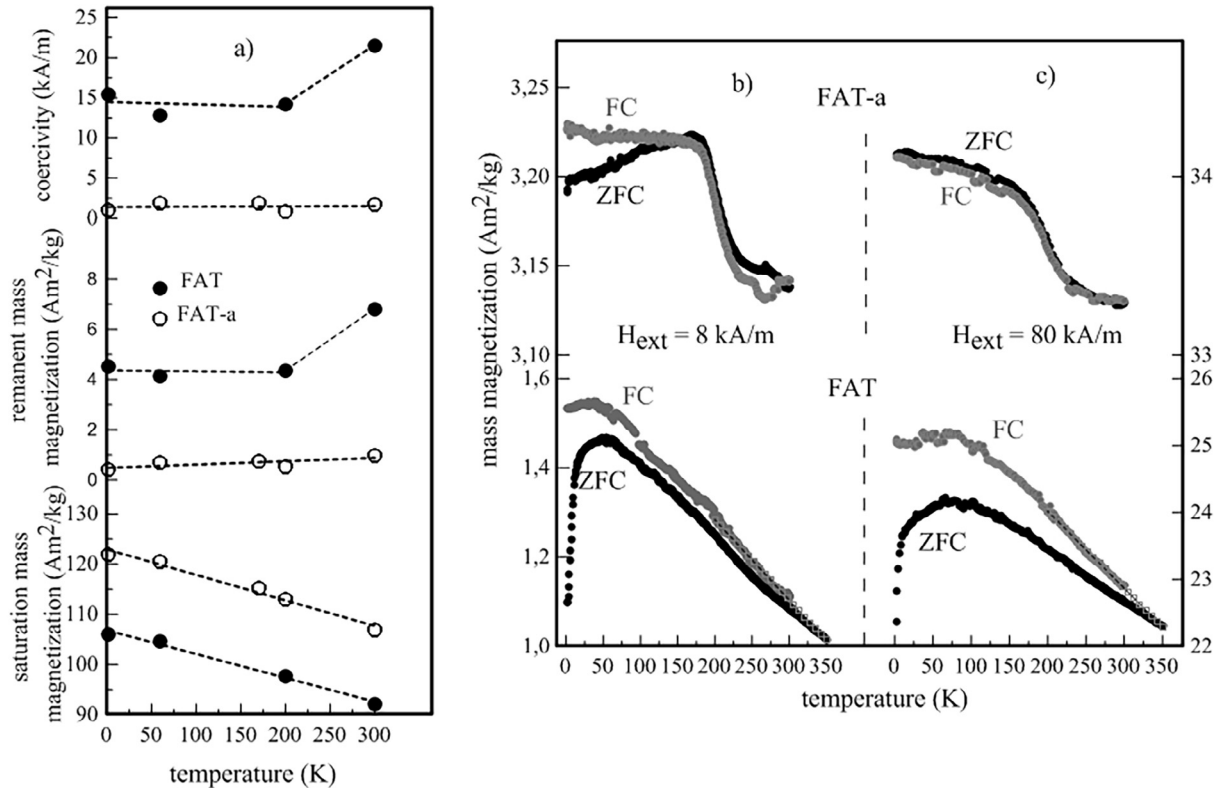

Fig. 9. Low temperature dependences of magnetic parameters (a) and zero-field-cooled (ZFC, black points) and field-cooled (FC, gray points) magnetizations measured in the external fields of 8 kA/m (b) and of 80 kA/m (c) of the Fe-Al-Ti as-prepared (FAT) and annealed (FAT-a) samples.

4.4. Mössbauer spectrometry

The experimental points (+) in Fig. 10 obtained by measurement of the Fe-Al and Fe-Al-Ti samples in the as-prepared (upper) and annealed (bottom) states using backscattered γ-rays were fitted by the CONFIT program allowing one to resolve the spectra into a set of sextuplets (FA) and into a set of sextuplets including single- and/or double-line components (FAT). The sum of all sub-components is represented by full lines (Fig. 10). Moreover, the spectra of the Fe-Al samples were evaluated by the above mentioned software using the direct fitting of theoretical atomic order models. The proper results were obtained by supposing the bcc-Fe lattice randomly occupied by Al atoms (*A2* ordering) combined with $D0_3$ superstructure for both FA and FA-a samples. The model spectra which do not include any type of defects are depicted in Fig. 10 left by pattern (▒). The agreement of both analyzing procedures is satisfactory and the mean values of hyperfine induction and isomer shift summarized in Table 3 are consistent with literature [35]. The analysis using the model yielded that about 19.9% of the FA sample is ordered into the $D0_3$ structure while the degree of ordering has increased to 64.9% after the thermal treatment. These results corroborate those of XRD, although both values are somewhat higher (see Table 1). This is due to a different sensitivity of both experimental methods. While the Mössbauer effect is highly sensitive to the local surrounding of resonating atoms and the same surroundings contribute to a particular component in the Mössbauer spectrum, the X-ray diffraction pattern reflects the coherent volumes with translation symmetry of the crystalline structure.

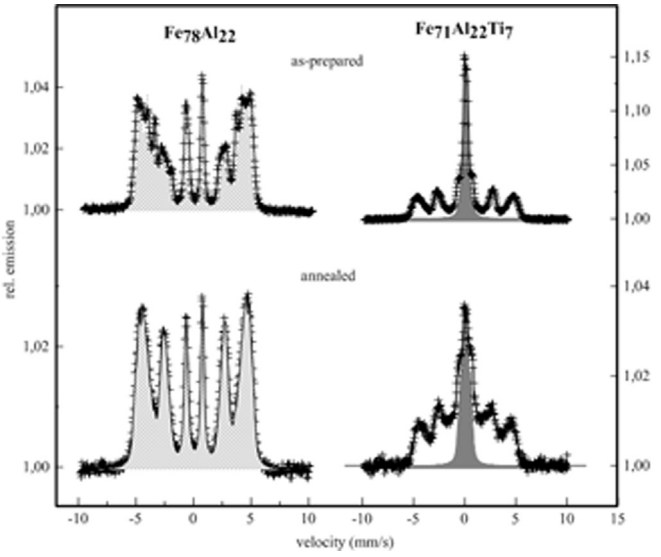

Fig. 10. Mössbauer spectra of the $Fe_{78}Al_{22}$ (left) and $Fe_{71}Al_{22}Ti_7$ (right) samples in the as-prepared and annealed states; experimental points (+), CONFIT analysis (full line), model analysis (▒ FA); paramagnetic Fe_2TiAl phase (gray).

Several years ago Dubiel et al. [36] presented a linear correlation between the mean values of the hyperfine field and the isomer shift. This was later also confirmed by Frackowiak [35]. Based on their findings, the mean values of hyperfine induction ~27 T and isomer shift ~0.09 mm/s correspond to the average number of Al atoms, $N_{Al} = 3.23$ in the first two nearest neighbor shells of the ^{57}Fe resonating

Table 3
Mean values of hyperfine induction B_{mean} and isomer shift δ_{mean}, obtained from the analysis of the Mössbauer data of the Fe-Al sample in the as-prepared (FA) and annealed (FA-a) state.

$Fe_{78}Al_{22}$		FA	FA-a
CONFIT	B_{mean} (T)	26.91 ± 0.16	27.13 ± 0.15
	δ_{mean} (mm/s)	0.088 ± 0.005	0.086 ± 0.007
MODEL	B_{mean} (T)	26.86 ± 0.16	27.51 ± 0.14
	δ_{mean} (mm/s)	0.094 ± 0.008	0.081 ± 0.008

Table 4
Mean values of hyperfine induction, B_{mean}, and isomer shift, δ_{mean}, of the ferromagnetic (fmc) Fe-Al(Ti) phase and isomer shifts, δ, and quadrupole splitting, Δ, of the paramagnetic (pmc) Fe_2TiAl phase. *RA* is the relative representation of the components.

$Fe_{71}Al_{22}Ti_7$		FAT	FAT-a
Fmc phase high-field	B_{mean} (T)	26.45 ± 0.16	24.51 ± 0.16
	δ_{mean} (mm/s)	0.107 ± 0.008	0.097 ± 0.009
	RA (%)	54.9 ± 0.6	61.8 ± 0.9
fmc phase low-field	B_{mean} (T)	4.98 ± 0.14	8.08 ± 0.012
	δ_{mean} (mm/s)	0.096 ± 0.014	0.085 ± 0.017
	RA (%)	5.7 ± 0.6	16.6 ± 0.2
pmc phase	δ_{D1} (mm/s)	0.141 ± 0.007	0.085 ± 0.005
	Δ_{D1} (mm/s)	0.296 ± 0.007	0.366 ± 0.015
	RA_{D1} (%)	26.9 ± 0.7	11.5 ± 0.6
	δ_{D2} (mm/s)	0.129 ± 0.004	0.128 ± 0.009
	Δ_{D2} (mm/s)	0.508 ± 0.003	0.953 ± 0.021
	RA_{D2} (%)	4.1 ± 0.1	5.8 ± 0.4
	δ_L (mm/s)	0.108 ± 0.002	0.071 ± 0.007
	RA_L (%)	8.4 ± 0.3	4.3
	$RA_{D1+D2+L}$(%)	39.4	21.6

atoms. Retroactively, the Al concentration $c_{Al} = (N_{Al}/14) \times 100 = 23.07$ at.% is in good agreement with the above presented result of the EDX analysis.

The spectra analyses of the Fe-Al-Ti as-prepared, FAT, and annealed, FAT-a, samples have to be done using the fmc and pmc components. According to Ref. [16] the pmc components are visible in the RT Mössbauer spectra for titanium contents above 3 at.%. Bellow this limit titanium is dissolved in the Fe-Al phase and it contributes to broadening of peaks. The pmc component is described by the single line (L) and the quadrupole doublets (D1, D2) of parameters seen in Table 4. The sum of the pmc sub-components is shown as a gray coloured spectrum besides the sum of six-line fmc sub-components (Fig. 10 right) which consists of two fmc parts, the high-field ($B_{mean} > 20$ T) and the low-field ($B_{mean} < 10$ T) detected in the spectra of FAT and FAT-a samples. Contrary to the FA sample the annealing of the FAT sample induces not only substantial differences of the macroscopic magnetic properties but also changes in representation of the individual phases and their hyperfine parameters owing to an atom reordering as seen in Table 4.

Assuming that the pmc P1 phase (Table 4) represents the Heusler Fe_2TiAl phase, then the fmc P2 intergrain Fe-Al phase should be slightly enriched by Fe, which yields an approximate concentration $Fe_{79}Al_{21}$. Considering the results published in Refs. [35,36], the mean value of the hyperfine induction for the FAT sample should be about 27 T. The obtained value, 26.45 T is slightly lower which can be due to a low content of Ti (< 3 at.% [16]) in the P2 phase detected by the EDX analysis. More complicated phase composition is obtained by analysis of Mössbauer spectrum of the FAT-a sample as it follows from Table 4. The mean value of hyperfine induction of the low-field magnetic component has increased as well as its representation in the whole spectrum above all at the expense of the pmc component. Based on some literature data [37,38] it could be that this fmc low-field component represents the $Ti_x(Fe,Al)_{100-x}$ Laves phase. This could contribute to explanation of the low-temperature magnetic behaviour of the FAT-a sample and of the detected magnetic transition temperature slightly above 200 K (Fig. 9 right panel). The sporadic magnetic studies of Fe-Al-Ti alloys of different compositions and a lack of the Mösbauer data for this system as a whole and especially for the Heusler Fe_2TiAl and/or Laves phases do not allow one to draw more specific conclusions at present; these facts call for the next more detailed investigations.

5. Conclusions

Present investigations are devoted to the Fe-22 at.% Al alloy modified by Ti at the expense of Fe. The obtained structural and physical properties are compared with those of the parent Fe-22 at.% Al alloy. The SEM, TEM, XRD, magnetic, and Mössbauer results have shown that the addition of 7 at.% Ti resulted in a substantially different microstructure compared to the original binary alloy. The produced nano-sized cuboids of the Heusler Fe_2TiAl phase embedded in the bcc-Fe-Al (Ti) matrix have influenced both microscopic hyperfine parameters and macroscopic magnetic characteristics. The as-prepared FeAlTi (FAT) samples yielded a lower saturation magnetization and were magnetically harder compared to the unmodified FeAl (FA) sample. These facts are explained by the paramagnetic behaviour of the Fe_2TiAl phase in the cuboid form. The structural and magnetic characteristics are highly sensitive to thermal treatment. The annealing at temperature 1273 K for 168 h has evoked an increase in the crystallite size from about 45–457 nm, a substantial atomic reordering, and changes in the phase composition. These effects were reflected in the magnetic softening and in the low-temperature magnetic behaviour of the sample. These features are corroborated by the Mössbauer phase analysis proving presence of a minor phase with the hyperfine induction of about 5 T in the as-prepared FAT sample. The content of this phase and its hyperfine induction have increased mainly at the expense of the paramagnetic Fe_2AlTi phase after the thermal treatment. Based on the low-temperature magnetic results and sporadic existing literature data, this phase has been speculatively identified as a $Ti_x(Fe,Al)_{100-x}$ Laves phase.

The obtained results contribute to the little explored area of the influence of Ti alloying on structural and magnetic properties of Fe-Al system. Nevertheless, a number of unclear points, related especially to the Heusler Fe_2TiAl phase, remain a subject for future studies.

Acknowledgements

This work was supported by the projects, 17-22139S funded by the Czech Science Foundation, LQ1601 (CEITEC 2020 – National Sustainability Programme II) and SP2018/43 both funded by Ministry of Education, Youth and Sports of the Czech Republic, VEGA 2/0082/17 and APVV-15-0049 both funded by the Slovak research and development agency. Special thanks are given to M. Hapla (IPM Brno) for the magnetic measurements and to I. Turek (IPM Brno) for fruitful discussions.

Appendix A. Supplementary data

Supplementary data associated with this article can be found, in the online version, at https://doi.org/10.1016/j.jmmm.2018.07.065.

References

[1] H.P. Longworth, D.E. Mikkola, Mater. Sci. Eng. 96 (1987) 213–229.
[2] I. Ohnuma, C.G. Schön, R. Kainuma, G. Inden, K. Ishida, Acta Mater. 46 (1998) 2083–2094.
[3] S.-M. Zhu, K. Sakamoro, M. Tamura, K. Iwasaki, Mater. Trans. 42 (2001) 484–490.
[4] T. Moriya, H. Nakashima, Y. Isokane, T. Miyazaki, T. Kozakai, T. Koyama, J. Phys. Soc. Jpn. 65 (1996) 293–296.
[5] R. Krein, M. Palm, J. Mater. Res. 24 (2009) 3412–3421.
[6] Y. Nishino, B.J. Inkson, T. Ogawa, C.J. Humphreys, Phil. Mag. Lett. 78 (1998) 97–103.
[7] M. Palm, G. Sauthoff, Intermetallics 12 (2004) 1345–1359.
[8] L.T.F. Eleno, L.A. Errico, P.G. Gonzales-Ormeno, H.M. Petrilli, C.G. Schön, Thermochemistry 44 (2014) 70–80.
[9] T. Komatsu, Y. Sakemi, K. Shimagami, K. Matusita, M. Miyazaki, J. Mater. Sci., Mater. Electron. 7 (1996) 101–106.
[10] C.G. McKamey, J.A. Horton, Metall. Trans. A Phys. Metall. Mater. 20 (1989) 751–757.
[11] T. Zak, J. Magn. Magn. Mater. 41 (1984) 47–48.
[12] P.G. Gonzales-Ormeno, R.N. Nogueira, C.G. Schön, H.M. Petrilli, Calphad-Comput. Coupling Ph. Diagr. Thermochem. 29 (2005) 222–229.
[13] C. Heck, Magnetische Werkstoffe und ihre technische Anwendung, Die Eisen-Aluminium-Legierungen, Dr. Alfred Hutehig Verlag GmbH, Heidelberg, 1967, p. 307.
[14] S.M. Zhu, K. Sakamoto, M. Tamura, K. Iwasaki, Mater. Trans. 42 (2001) 484–490.
[15] A. Michalcova, L. Sencekova, G. Rolink, A. Weisheit, J. Pesicka, M. Stobik, M. Palm, Mat. Des. 116 (2017) 481–494.

[16] G. Athanassiadis, G. Le Caer, J. Foct, R. Rimlinger, Phys. Stat. Sol. (a) 40 (1977) 425–435.
[17] M.G. Mendiratta, S.K. Ehlers, H.A. Lipsitt, Metall. Trans. 18A (1987) 509–518.
[18] R. Krein, M. Friak, J. Neugebauer, M. Palm, M. Heilmaier, Intermetallics 18 (2010) 1360–1364.
[19] R.A. Young, The Rietveld Method, International Union of Crystallography Oxford University Press, Oxford, 1993.
[20] ICSD Database, Version 1.9.4., 2014-1, NIST/FIZ.
[21] T. Zak, Y. Jiraskova, Surf. Interface Anal. 38 (2006) 710–714.
[22] V. Paidar, Czech J. Phys. B 23 (1973) 454–461.
[23] T. Žák, IEEE Trans. Magn. 20 (1984) 1454–1456.
[24] P.R. Alonso, P.H. Gargano, P.B. Bozzano, G.E. Ramirez-Caballero, P.B. Balbuena, Intermetallics 19 (2011) 1157–1167.
[25] C.H. Sellers, T.A. Hyde, T.K. ÓBrien, R.N. Wright, J. Phys. Chem. Solids 55 (1994) 505–515.
[26] L.T.F. Eleno, L.A. Errico, P.G. Gonzales-Ormeño, H.M. Petrilli, C.G. Schön, Calphad-Comput. Coupling Ph. Diagr. Thermochem. 44 (2014) 70–80.
[27] K. Brzakalik, J.E. Frackowiak, Nukleonika 48 (Suppl. 1) (2003) S13–S16.
[28] K.H.J. Buschow, P.G. van Engen, J. Magn. Magn. Mater. 25 (1981) 90–96 P.G.
[29] F. Stein, M. Palm, Int. J. Mat. Res. 98 (2007) 580–588.
[30] H. Sato, A. Arrot, Phys. Rev. 114 (1959) 1427–1440.
[31] G. Herzer, Nanocrystalline soft magnetic alloys, Elsevier Science B.V., 1997, p. 478.
[32] P.A. Beck, Metall. Trans. 2 (1971) 2015.
[33] R. Nathans, M.T. Pigott, C.G. Shull, J. Phys. Chem. Solids 6 (1958) 38–42.
[34] E. Shreder, S.V. Streltsov, A. Svyashin, A. Makhnev, V.V. Marchenkov, A. Lukayanov, H.W. Weber, J. Phys. Condens. Matter 20 (2008) 0452127pp.
[35] J.E. Frackowiak, Hyperfine Interact. 54 (1990) 793–798.
[36] S.M. Dubiel, W. Zinn, Phys. Rev. B 26 (1982) 1574–1589.
[37] K. Sumiyama, H. Yasuda, Y. Nakamura, J. Phys. Condens. Matter 2 (1990) 3595–3610.
[38] E.F. Wassermann, B. Rellinghaus, Th. Roessel, W. Pepperhoff, J. Magn. Magn. Mater. 190 (1998) 289–301.